Synthetic Metals 210 (2015) 304–313

Contents lists available at ScienceDirect

Synthetic Metals

journal homepage: www.elsevier.com/locate/synmet

Low band gap polymer consisting of quinacridone and diketopyrrolopyrrole and isoindigo units: correlation of ordered structure and intramolecular charge transfer properties

Doo Hun Kim[a], Ho Jun Song[b], Eui Jin Lee[a], Eui Jin Ko[a], Doo Kyung Moon[a,*]

[a] Department of Material Chemistry and Engineering, Konkuk University, Seoul 143-701, Republic of Korea
[b] Cungcheong Regional Division IT Convergence Material R&D Group, Korea Institute of Industrial Technology, 89 Yangdaegiro-gil, Ipjang-myeon, Seobuk-gu, Cheonan-si, Chungcheongnam-do 331-822, Republic of Korea

ARTICLE INFO

Article history:
Received 27 July 2015
Received in revised form 9 October 2015
Accepted 12 October 2015
Available online 4 November 2015

Keywords:
Low-band gap polymer
OPVs
Quinacridone
Diketopyrrolopyrrole
Iso-Indigo

ABSTRACT

Demand for low band gap polymer materials is driven by the fast growing organic photovoltaic industry. In the present study, to develop highly functional conjugated polymers, poly[quinacridone-diketopyrrolopyrrole] (PQCDPP) and poly[quinacridone-isoindigo] (PQCDIG) were synthesized via the Suzuki coupling reaction. While these two polymers provided high absorption in the region of over 700 nm, PQCIDG had broader absorption across the visible spectrum (300–600 nm) than PQCDPP because a greater intramolecular charge transfer occurs between the quincaridone and isoindigo units. Based on X-ray diffraction (XRD) results, large factions of the two polymers exhibited a face-on orientation with respect to the substrate, and the orientation distributions of 24.5° were more dominant in PQCIDG, compared with PQCDPP. In this study, we fabricated enhanced-polymer-based bulk-heterojunction (BHJ) solar cells using a normal structure of ITO/PEDOT:PSS/active-layer/Al and assessed its performance in terms of photovoltaic characteristics. The PQCIDG-based devices (polymer/$PC_{71}BM$ = 1:3) showed power conversion efficiency (PCE) of 2.7% with open circuit voltage (V_{oc}) of 0.83 V, short circuit current (J_{sc}) of 7.4 mA/cm^2 and fill factor (FF) of 43.1%.

1. Introduction

Semiconducting polymers are used in a wider range of applications, including organic light emitting diodes(OLEDs), [1–3] organic photovoltaic cells (OPVs) [4–9], organic thin film transistors (OTFTs) [10–12]. In particular, polymer application in photovoltaic cells (OPV) draws international attention for promising results, associated with its environment-friendly and cost-effectiveness advantages. Bulk heterojunction (BHJ) polymer solar cells (PSC) hold great promise because of low-cost fabrication, roll-to-roll processing and large area coverage, and the optimization of molecular structure of polymers is a crucial step in achieving the desired photovoltaic performance of PSC. Conjugated polymers are considered ideal when they meet the following criteria: (1) low band gap for wide absorption spectrum (2) crystallite structure to achieve good charge transport (3) low highest occupied molecular orbital (HOMO) energy level to achieve high V_{oc} and (4) appropriate lowest unoccupied molecular orbital (LUMO) energy levels required for effective electron transfer to fullerene.

As a way of reducing the band gap, electron withdrawing properties of the acceptor can be incorporated into the main chain of the polymer to construct a donor (D)–acceptor (A) (D–A) type. The D–A type low band gap polymers provide great potential because it is easy to improve their electron properties for a wider absorption spectrum by modifying unique D–A characteristics [13].

Diketopyrrolopyrrole (DPP) and isoindigo (IDG) pigments are widely used as a strong acceptor of D–A conjugated polymers [14–16].

All DPP compounds are flat in an ordered structure, and strong π–π interaction of polymer chains becomes possible, enabling charge delocalization and intramolecular charge hopping for effective carrier mobility [17]. Yang et al. claimed a very high hole mobility of 12.25 cm^2 V^{-1} s^{-1} by applying DPP derivatives (ε-chain) as an acceptor to OFET and modifying intramolecular π–π interactions [18].

The IDG-based polymers reportedly have a wide absorption spectrum, low-lying HOMO (−5.30 to −5.90 V) and LUMO (−3.70 to −4.00 V), indicating a low band gap ranging from 1.3 to 1.8 [16]. Peng et al. introduced a new D–A type polymer by synthesizing fluorinated isoindigo after inserting fluorine atoms into IDG. They claimed the D–A type polymers had a band-gap of

* Corresponding author. Fax: +82 2 444 0765.
E-mail address: dkmoon@konkuk.ac.kr (D.K. Moon).

http://dx.doi.org/10.1016/j.synthmet.2015.10.009
0379-6779/

1.6 and UV absorption spectrum of 300–800. Also, they found a shoulder peak resulted from fluorine-induced aggregation between polymer backbones [19].

Quinacridone(QC) derivatives, which are known as red-violet pigments, are also used as OTFTs material because their high crystallinity and unique self-assembly increase hole mobility. However, small molecules and oligomer forms of QC derivatives limit their use for polymers. Recently, Takimiya et al. unveiled novel QC derivative-based polymers that have high hole mobility of 0.2 $cm^2 V^{-1} s^{-1}$ and are designed for use in OTFTs [20].

In this study, we employed DPP, IDG derivatives and QC derivatives to synthesize two novel polymers of poly[quinacridone-diketopyrrolopyrrole](PQCDPP) and poly[quinacridone-isoindigo](PQCIDG). These synthetic polymers are characterized by strong electron-withdrawing, wide absorption spectrum and strong intramolecular charge transfer. The structure and properties of the synthetic polymers were characterized and compared. The efficiency of BHJ devices fabricated using these polymers and $PC_{71}BM$ (3′H-cyclopropa[8,25][5,6]fullerene-C70-D5h(6)-3′-butanoic acid, 3′-phenyl-, methyl ester) was also assessed.

2. Experimental

2.1. Instruments and characterization

Unless otherwise specified, all the reactions were carried out under nitrogen atmosphere. Solvents were dried by standard procedures. All column chromatography was performed with the use of silica gel (230–400 mesh, Merck) as the stationary phase. 1H-NMR spectra were performed in a Bruker ARX 400 spectrometer using solutions in $CDCl_3$ and chemical were recorded in ppm units with TMS as the internal standard. The elemental analyses were measured with EA1112 using a CE Instrument. Electronic absorption spectra were measured in chloroform using a HP Agilent 8453 UV–vis spectrophotometer. The cyclic voltammetric waves were produced using a Zahner IM6eX electrochemical workstation with a 0.1 M acetonitrile (substituted with nitrogen for 20 min) solution containing tetrabutyl ammonium hexafluorophosphate (Bu_4NPF_6) as the electrolyte at a constant scan rate of 50 mV/s. ITO, a Pt wire, and silver/silver chloride [Ag in 0.1 M KCl] were used as the working, counter, and reference electrodes, respectively. The electrochemical potential was calibrated against Fc/Fc+. The HOMO levels of the polymers were determined using the oxidation onset value. Onset potentials are values obtained from the intersection of the two tangents drawn at the rising current and the baseline changing current of the CV curves. TGA measurements were performed on NETZSCH TG 209 F3 thermogravimetric analyzer. All GPC analyses were made using THF as eluant and polystyrene standard as reference. X-ray diffraction (XRD) patterns were obtained using SmartLab 3 kW (40 kV 30 mA, Cu target, wavelength: 1.541871 ang), Rigaku, Japan. Topographic images of the active layers were obtained through atomic force microscopy (AFM) in tapping mode under ambient conditions using a XE-100 instrument.

2.2. Fabrication and characterization of polymer solar cells

All of the bulk-heterojunction PV cells were prepared using the following device fabrication procedure. The glass/indium tin oxide (ITO) substrates [Sanyo, Japan (10 Ω/γ)] were sequentially lithographically patterned, cleaned with detergent, and ultrasonicated in deionized water, acetone, and isopropyl alcohol. Then the substrates were dried on a hot-plate at 120 °C for 10 min and treated with oxygen plasma for 10 min in order to improve the contact angle just before the film coating process. Poly(3,4-ethylene-dioxythiophene): poly(styrene-sulfonate) (PEDOT:PSS, Baytron P 4083 Bayer AG) was passed through a 0.45 μm filter before being deposited onto ITO at a thickness of ca. 32 nm by spin-coating at 4000 rpm in air and then it was dried at 120 °C for 20 min inside a glove box. Composite solutions with polymers and PCBM were prepared using 1,2-dichlorobenzene (DCB) or chlorobenzene (CBz). The concentration was controlled adequately in the 0.5 wt% range, and the solutions were then filtered through a 0.45 μm PTFE filter and then spin-coated (500–2000 rpm, 30 s) on top of the PEDOT:PSS layer. The device fabrication was completed by depositing thin layers of Al (100 nm) at pressures of less than 10^{-6} torr. The active area of the device was 4.0 mm^2. Finally, the cell was encapsulated using UV-curing glue (Nagase, Japan). In this study, all of the devices were fabricated with the following structure: ITO glass/PEDOT:PS/polymer:PCBM/Al/encapsulation glass. The illumination intensity was calibrated using a standard a Si photodiode detector that was equipped with a KG-5filter. The output photocurrent was adjusted to match the photocurrent of the Si reference cell in order to obtain a power density of 100 mW/cm^2. After the encapsulation, all of the devices were operated under an ambient atmosphere at 25 °C. The current–voltage (*I–V*) curves of the photovoltaic devices were measured using a computer-controlled Keithley 2400 source measurement unit (SMU) that was equipped with a Peccell solar simulator under an illumination of AM 1.5G (100 mW/cm^2). Thicknesses of the thin films were measured using a KLA Tencor Alpha-step 500 surface profilometer with an accuracy of 1 nm. Hole-only devices were fabricated with a diode configuration of ITO (170 nm)/PEDOT:PSS (40 nm)/polymer:$PC_{71}BM$ (34–110 nm)/MoO_3 (30 nm)/Al (100 nm). The hole mobilities of the active layers were calculated from the SCLC using the *J*–V curves of the hole only devices in the dark as follows:

$$J = \frac{9}{8}\varepsilon_r \varepsilon_0 \mu_{h(e)} \frac{V^2}{L^3} \exp\left(0.89\sqrt{\frac{V}{E_0 L}}\right)$$

where ε_0 is the permittivity of free space (8.85×10^{-14} C/Vcm); ε_r is the dielectric constant (assumed to be 3, which is a typical value for conjugated polymers) of the polymer; $\mu_{h(e)}$ is the zero-field mobility of holes (electrons); L is the film thickness; and $V = V_{appl} - (V_r + V_{bi})$, where V_{appl} is the voltage applied to the device, V_r is the voltage drop due to series resistance across the electrodes and V_{bi} is the built-in voltage.

2.3. Materials

All reagents were purchased from Aldrich, Acros or TCI companies. All chemcals were used without further purification. The following compound were synthesized following modified literature procedures: *N*,*N*′-di(2-octyldodecyl) quinacridone (QC-1), 2,9-dibromo-*N*,*N*′-di(2-octyldodecyl) quinacridone. (QC-2), 5,12-bis(2-octyldodecyl)-2,9-bis(4,4,5,5-tetramethyl-1,3,2-dioxaborolan-2-yl) quinolino[2,3-b]acridine-7,14(5H,12H)-dione (M1) [21], 3,6-bis(5-bromothiophen-2-yl)-2,5-bis(2-hexyldecyl) pyrrolo[3,4-c]pyrrole-1,4(2H,5H)-dione (M2) [9], isoindigo (M3) [22].

2.4. Poly[quincaridone- diketopyrrolopyrrole] (PQCDPP)

5,12-Bis(2-octyldodecyl)-2,9-bis(4,4,5,5-tetramethyl-1,3,2-dioxaborolan-2-yl) quinolino[2,3-b]acridine-7,14(5H,12H)-dione (M1) (0.23 g, 0.20 mmol), 3,6-bis(5-bromothiophen-2-yl)-2,5-bis (2-hexyldecyl) pyrrolo[3,4-c]pyrrole-1,4(2H,5H)-dione (M2) (0.18 g, 0.20 mmol) Pd(PPh3) 4(0) (0.007 g, 0.006 mmol) and aliquat 336 were placed in a Schlenk tube, purged by performing three nitrogen/vacuum cycles and, under a nitrogen atmosphere,

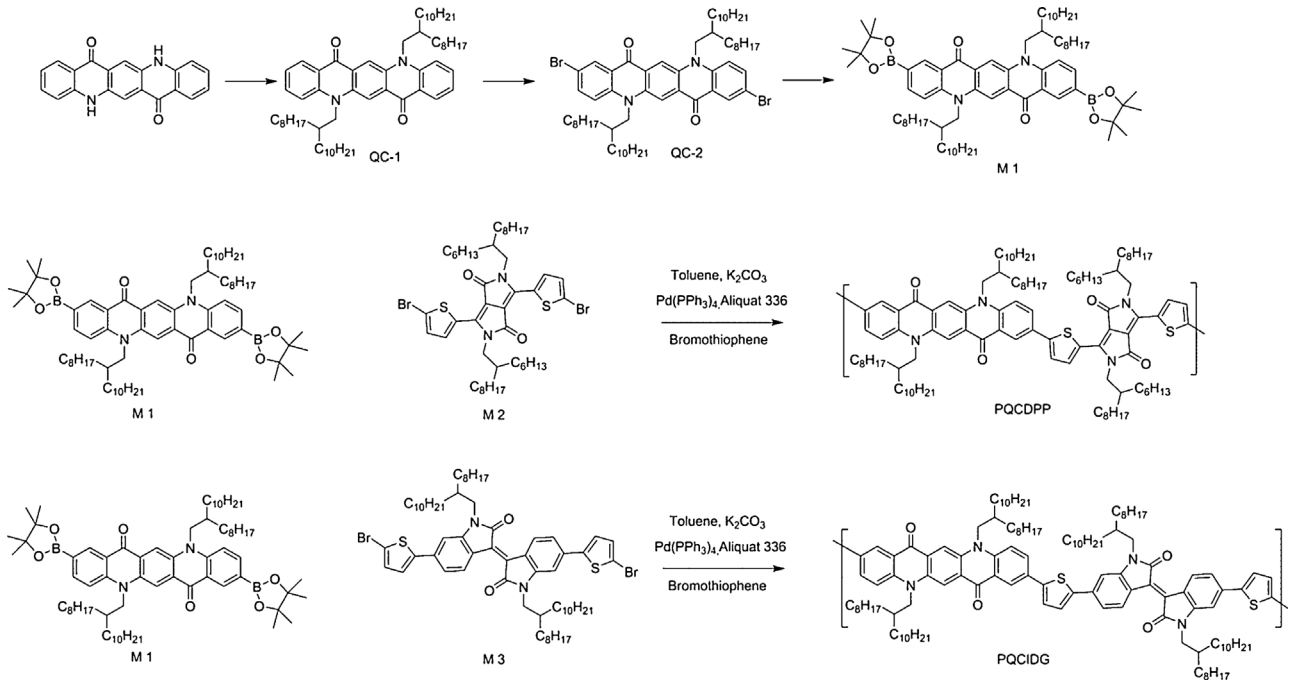

Scheme 1. Scheme of monomer synthesis and polymerization.

added with 2 M degassed aqueous K_2CO_3 (10 mL) and dry toluene (20 mL). The mixture was heated to 90 °C and stirred in the dark for 24 h. Following polymerization, the polymer was end-capped with bromothiophene. After quenching the reaction, the entire mixture was poured into methanol. The precipitate was filtered off and purified by Soxhlet extraction in the following order: methanol, acetone and chloroform. The polymer was recovered from the chloroform fraction and precipitated in methanol. The final product was obtained after drying in vacuum. Dark purple solid. (0.29 g, 89%) Anal. Calcd for $C_{106}H_{162}N_4O_4S_2$: C, 78.56; H, 10.08; N, 3.46; S, 3.95; O, 3.96. Found: C, 78.05; H, 10.03; N, 3.49; S, 3.88; O, 4.53.

2.5. Poly[quinacridone-isoindigo] (PQCIDG)

5,12-Bis(2-octyldodecyl)-2,9-bis(4,4,5,5-tetramethyl-1,3,2-dioxaborolan-2-yl) quinolino[2,3-b]acridine-7,14(5H,12H)-dione (M1) (0.25 g, 0.22 mmol), isoindigo (M3) (0.25 g, 0.22 mmol) Pd (PPh3) 4(0) (0.008 g, 0.007 mmol) and aliquat336 were placed in a Schlenk tube, purged by performing three nitrogen/vacuum cycles and, under a nitrogen atmosphere, added with 2 M degassed aqueous K_2CO_3 (10 mL) and dry toluene (20 mL). The mixture was heated to 90 °C and stirred in the dark for 24 h. Following polymerization, the polymer was end-capped with bromothiophene. After quenching the reaction, the entire mixture was poured into methanol. The precipitate was filtered off and purified by Soxhlet extraction in the following order: methanol, acetone and chloroform. The polymer was recovered from the chloroform fraction and precipitated in methanol. The final product was obtained after drying in vacuum. Dark purple solid. (0.24 g, 59%) Anal. Calcd for $C_{124}H_{184}N_4O_4S_2$: C, 80.12; H, 9.98; N, 3.01; S, 3.45; O, 3.44. Found: C, 79.21; H, 9.86; N, 2.96; S, 3.22; O, 3.81.

3. Results & discussion

3.1. Material synthesis

Chemical composition of monomers and polymers and the polymerization process we followed are shown in Scheme 1: poly [quincaridone-diketopyrrolopyrrole] (PQCDPP) based on monomer quinacridone (M1), diketopyrrolopyrrole (M2) and poly [quinacridone-isoindigo] (PQCIDG) based on quinacridone (M1) and isoindigo (M3) were synthesized via the Suzuki coupling reaction.

Polymer synthesis was triggered by palladium catalyst (0), 2 M potassium carbonate solution, aliquat 336 (surfactant) and toluene (solvent) with reaction time of 24 h and heating to 90 °C. The polymerization process was followed by end-capping with boromothiophene. The end-capped polymers were then purified using soxhlet methanol, acetone and chloroform in sequence. The yields of PQCDPP and PQCIDG re-precipitated into methanol were 89% and 59%, respectively. These polymers were soluble in most organic solvents, including THF, chloroform, chlorobenzene and *o*-dichlorobenzene and processed into thin films via spin coating. The firms are purple, homogeneous and semi-transparent.

3.2. Molecular weight and thermal properties

Table 1 shows the molecular weight and thermal behaviors of the polymers. In Table 1, gel permeation chromatography (GPC)

Table 1
Molecular weight and thermal properties of the polymers.

Polymer	M_n (kg/mol)	M_w (kg/mol)	PDI	T_d (°C)[a]
PQCDPP	123.8	227.3	1.83	350
PQCIDG	44.9	175.8	3.91	356

[a] Temperature resulting in 5% weight loss based on initial weight.

analysis using polystyrene as the standard revealed the mean molecular weights of 123.8 and 44.9 kg/mol and polydispersity indices(PDI) of 1.83 and 3.91 for PQCDPP and PQCIDG, respectively. The degree of polymerization of PQCDPP was 2–3 times higher than other OPV polymers [7,21]. Table 1 shows the results performed by thermogravimetric analysis (TGA). In Fig. S1, both PQCDPP and PQCIDG exhibit high thermal stability of 350, 356 °C with a 5wt% loss because thermal degradation is prevented by rigid structure of QC derivative. Thus PQCDPP and PQCIDG have potential applications in polymer solar cells or optoelectronic devices that require thermal stability of over 300 °C [21,23]. Conjugation length increases with increasing molecular weight, leading to high photon absorption efficiency and subsequent generation of a high photocurrent.

3.3. Optical and electrochemical properties

In Fig. 1, UV–vis absorption spectra were measured for PQCDPP and PQCIDG in a chloroform solution (10^{-6} M) and in the spin-coated thin film (thickness of 50 nm). In solution, the absorption maximum of PQCDPP was $1.57 \times 10^5\,M^{-1}\,cm^{-1}$ at 696 nm and PQCIDG's absorption maximum was $4.51 \times 10^4\,M^{-1}\,cm^{-1}$ at 621 nm.

PQCDPP showed an absorption region of 350 nm to 750 nm, but absorption at 400–550 nm is very week in both solution and thin film states, and the wide absorption of PQCDPP was attributed to interchain aggregation. [24]

PQCIDG thin films showed an absorption spectrum of 350–450 nm, which originated from the π–π^* transition of the conjugated backbone. Its absorption band in the region between 500 and 750 originated from intramolecular charge-transfer (ICT) between donor and acceptor moieties. [25]

As compared to simulated spectra of QC, DPP and IDG, an enlargement of absorption ranges is observed which broaden the solar domain of the photons absorption. (describe in the ESI Fig. 2)

In the UV region, PQCDPP and PQCIDG films exhibited their band edge positions at 751 nm and 742 nm, respectively, indicating both a broad wavelength range and small optical band gaps.

Fig. 2 and Table 2 show the results of a cyclic voltammetry (CV) experiment performed to determine the HOMO and LUMO levels in PQCDPP and PQCIDGP films.

PQCDPP and PQCIDG exhibited oxidation onset potentials of +0.96 and 1.03, respectively, and HOMO levels of −5.31 eV and −5.38 eV, respectively. The LUMO energy levels of PQCDPP and PQCIDG, which were calculated by subtracting the HOMO value from the optical band gap, were −3.66 and −3.71, respectively.

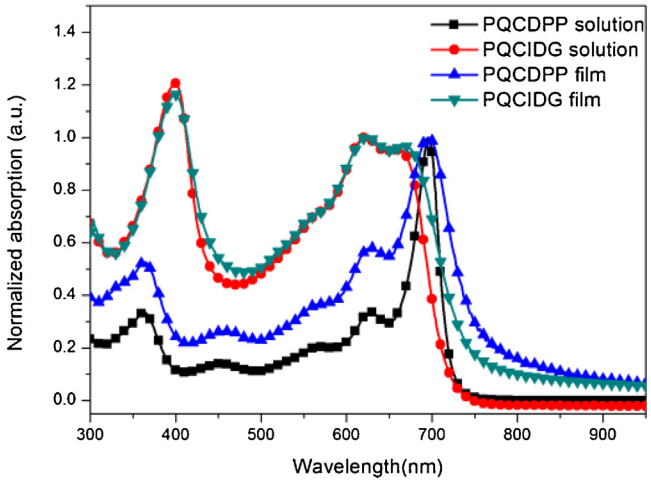

Fig. 1. Absorption spectra of polymers in solution & film.

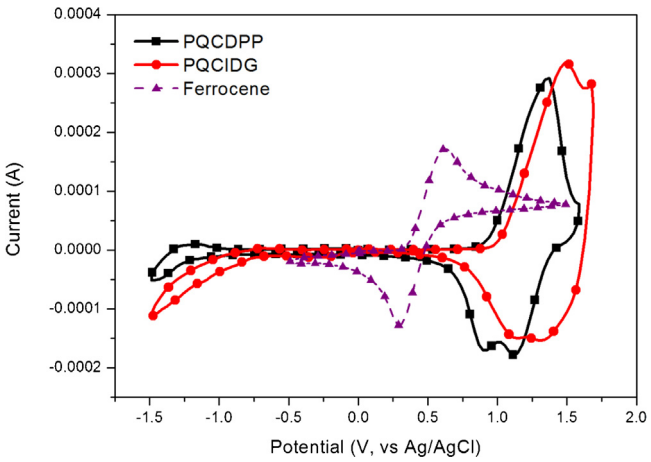

Fig. 2. Cyclic voltammogram of polymers.

The PQCIDG exhibited lower HOMO and LUMO levels than PQCDPP that contains same donor (QC) as a donor because the differences between the two polymers with respect to molecular energy levels are directly proportional to the difference between energy levels of the donor material (DPP) and the acceptor material (IDG). The HOMO–LOMO levels of DPP monomer were −5.3 eV and −3.4 eV, which were higher than −5.7 eV and −3.5 eV of IDG monomer, and the IDG monomer exhibited more low-lying frontier orbital than the DPP monomer. [26]

3.4. Computational study

In Fig. 3, density functional theory (DFT) was compared to characterize the intramolecular interaction and electron properties. Based on DFT calculations, the band structures of PQCDPP and PQCIDG were analyzed, and the resulting images show optimized molecular geometry with the number of a repeat unit ($n = 3$). The top and side view of the structure revealed the molecular shape of a trigonal planar, which is deemed to facilitate electron mobility in conjugated molecular geometry [27,28].

According to DFT calculations, the HOMO levels of PQCDPP and PQCIDG were −4.8 eV and −5.0 eV, while their LUMO levels were −2.4 eV and −2.7 eV. These levels were higher than the results of CV experiments, and this finding was consistent with other studies.

The distribution of an electron cloud of PQCDPP revealed electron density localized at the DPP unit as a result of the HOMO level was higher but the lower LUMO level was at the DPP unit, compared with the QC unit. This finding is similar with the electron behaviors of the PQADPP(poly[quinacridone-diketopyrrolopyrrole]) reported by Takimiya et al [29]. The distribution of electron cloud of PQCIDG, electrons were delocalized on all polymer chains in the HOMO level, and electron density was mainly observed at the IDG unit in the LUMO level [28]. As the HOMO levels of the two polymers were below the P3HT HOMO level (4.9 eV), air stability and open circuit voltage (V_{oc}) can be improved [30].

In Fig. 3, the LUMO levels of PQCIDG and $PC_{71}BM$ were 3.71 eV and 4.0 eV, respectively, showing a difference of 0.29 eV, which is the smallest difference, whereas its HOMO level (5.38 eV) was higher, it was as much as 0.39 eV higher than PEDOT:PSS HOMO level(5.0 eV). Therefore, the PQICDG-based device can effectively balance positive holes transferring from PQCIDG to PEDOT:PSS and negative electrons moving from PQCIDG to $PC_{71}BM$ when sunlight-induced charge separation occurs [31].

Table 2
Optical and electrochemical properties of the polymers.

Polymer	Absorption, λ_{max}(nm)		E_{ox}^{onset} (V)	E_{HOMO} (eV)[c]	E_{LUMO} (eV)[d]	E_{opt} (eV)[e]
	Solution[a]	Film[b]				
PQCDPP	363,696	363,696	0.96	−5.31	−3.66	1.65
PQCIDG	399, 621, 659	400,624,668	1.03	−5.38	−3.71	1.67

[a] Absorption spectrum in $CHCl_3$ solution (10^{-6} M).
[b] Spin-coated thin film (50 nm).
[c] Calculated from the oxidation onset potentials under the assumption that the absolute energy level of Fc/Fc+ was −4.8 eV below a vacuum.
[d] HOMO−E_{opt}.
[e] Estimated from the onset of UV–vis absorption data of the thin film.

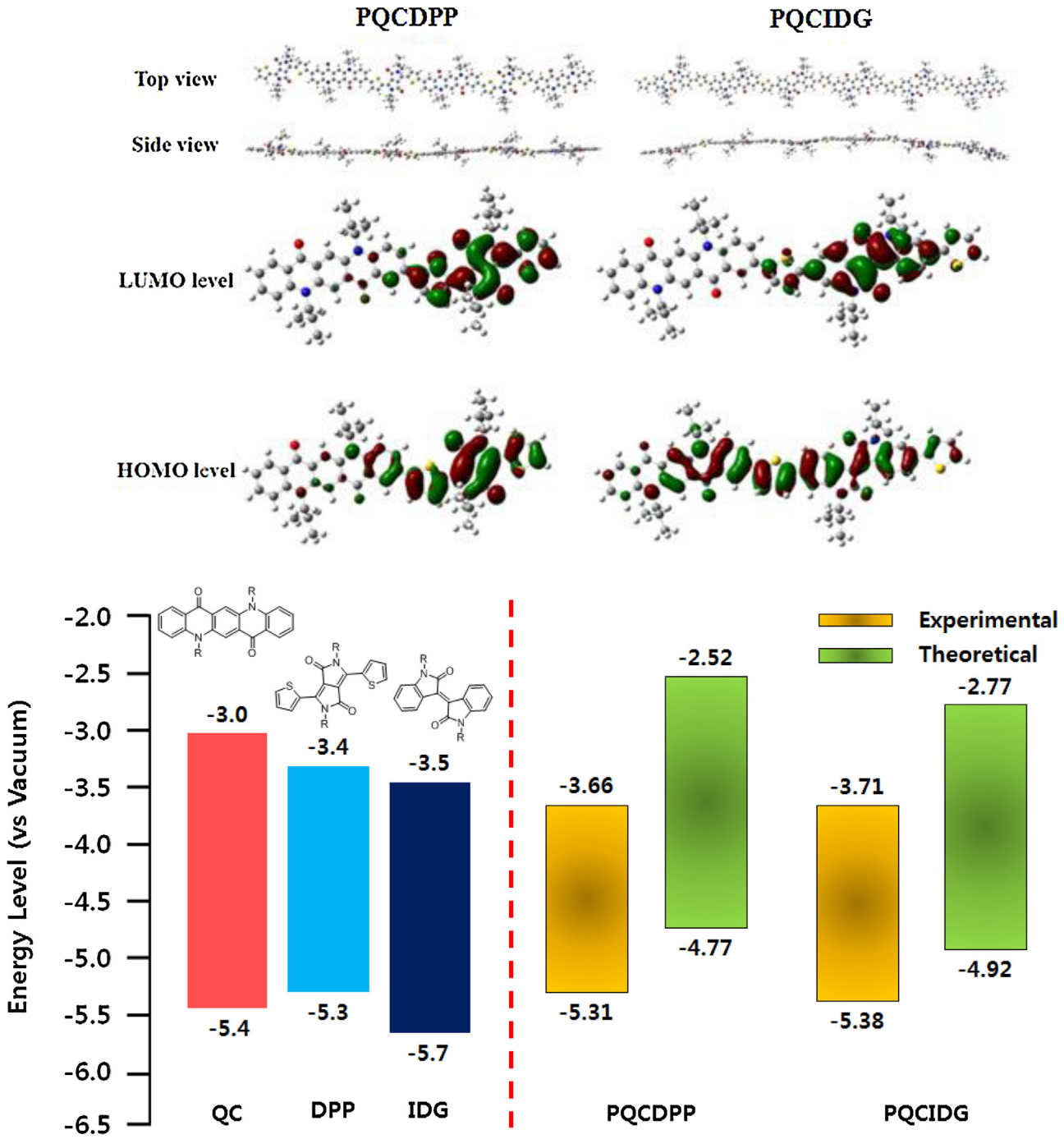

Fig. 3. DFT Gaussian simulation and Band diagram of polymers.

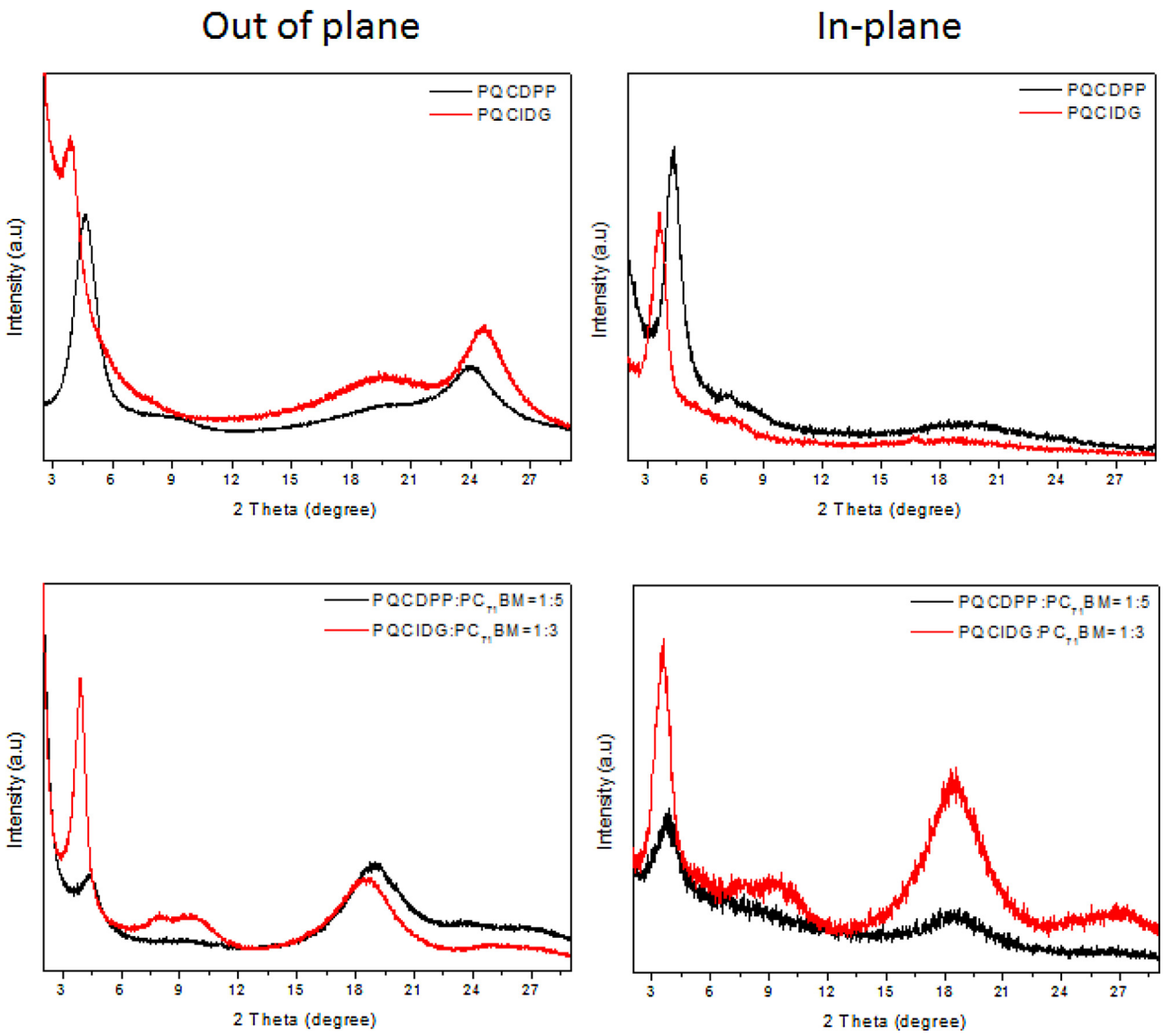

Fig. 4. Out-of-plane, in-plane image X-ray diffraction pattern of annealed polymer in thin films.

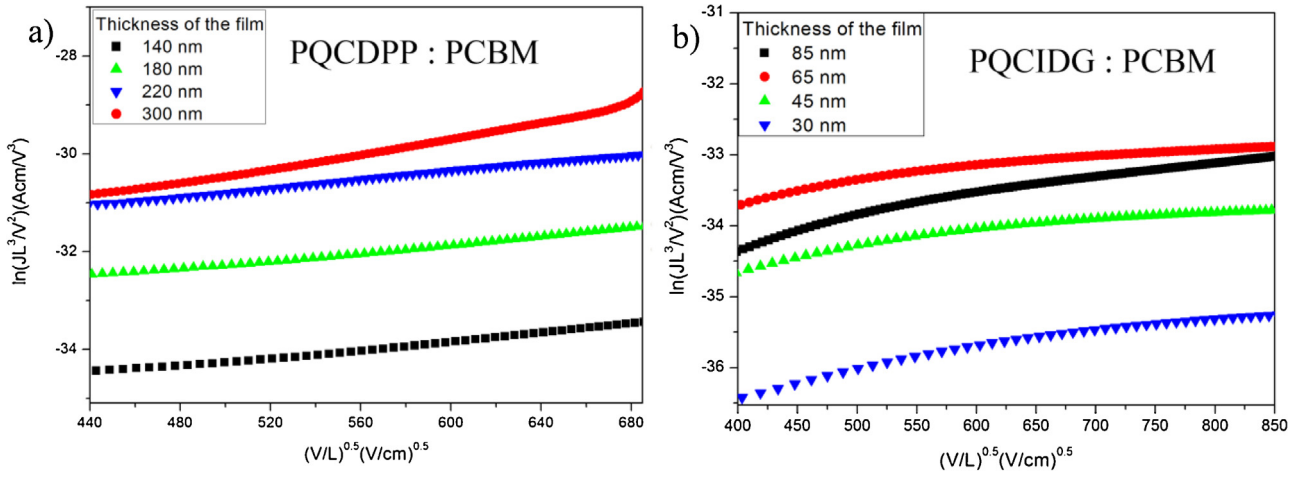

Fig. 5. hole-only devices and optimized molecular structure. (a) PQCDPP (b) PQCIDG.

Table 3
Hole mobility of polymers blended with $PC_{71}BM$.

Active layer	Film thickness [nm]	Hole mobility [$cm^2(V^{-1}s^{-1})$]
PQCDPP:$PC_{71}BM$ = 1:5	34	5.32×10^{-4}
	58.2	1.54×10^{-2}
	83.2	4.06×10^{-3}
	110	4.63×10^{-3}
–		
PQCIDG:$PC_{71}BM$ = 1:3	35	2.50×10^{-4}
	43.9	2.13×10^{-3}
	64.9	5.62×10^{-3}
	85.2	2.10×10^{-3}

3.5. Orientation analysis

In Fig. 4, the XRD pattern was measured to analyze the ordered structure of the polymers in solid states. The PQCDPP layer was fabricated by spin coating with the PQCDPP solution dissolved in the ODCB (10 mg/1 mL). The PQCIDG layer was fabricated by spin coating with the PQCIDG solution dissolved in the CB (10 mg/1 mL).

The out of plane mode of PQCDPP and PQCIDG diffraction patterns revealed two XRD peaks at 3.8° and 4.5°, forming a highly ordered lamellar structure (1 0 0). Also, broad diffraction peaks were observed in the XRD pattern around 24.0° and 24.5°, indicating the influence of π–π interactions (0 1 0) on crystal planes. The π–π stacking distance (d_π) of PQCDPP and PQCIDG was 3.71 and 3.63 Å ($\lambda = 2d\sin\theta$), respectively. These distance values were smaller than the pre-existing benzene-thiophene linkage d_π value of 4.0–4.4 Å.

When a π–π stacking peak is observed for the (0 1 0) plane in the out-of-plane mode, it is highly probable that the polymer thin film adopts a crystalline form with face-on orientation [32,33].

This result suggested that a large fraction of the PQCIDG backbones were oriented face-on relative to the substrate. In other words, the π-stacking direction was perpendicular to that of the substrate [34,35]. A parallel conjugated polymer backbone plane relative to the electrode surface and the effective π-stacking of the polymer backbones result in an efficient charge transport through interchain interactions and a relatively high carrier mobility [36].

The ordered structure of the polymer/ $PC_{71}BM$-based layer was also investigated by XRD. In the out of plane modes of the polymer: $PC_{71}BM$ layer, the areas of two peaks corresponding to fullerene crystallinity were prominently observed in the XRD pattern around 18.97°, 18.49.

By individual polymer, the PQCDPP: $PC_{71}BM$ layer exhibited an amorphous structure without lamellar and π–π scattering whereas the PQCIDG:$PC_{71}BM$ layer exhibited strong ordered lamellar scattering along with the intensity of (0 1 0) crystal plane attributable to π–π stacking

Overall, the PQCIDG-based film was more capable of boosting the photocurrent output and subsequent charge mobility. [32,33,37].

Dihedral angles were comparatively analyzed by calculating the PQCDPP, PQCIDG configurations using a DFT calculation. Dihedral angles between thiophene and quinacridone were 18–30° in PQCDPP and 12–24° in PQCIDG. The formation of a planar backbone was observed in PQCDPP and PQCIDG. Based on this result, it was confirmed that π–π stacking was more effective in PQCIDG than in PQCDPP due to the steric hindrance of the DPP unit that was introduced to the main chain of PQCDPP.

3.6. Charge carrier mobility

Fig. 5 and Table 3 shows *J–V* characteristics of PQCDPP:$PC_{71}BM$- and PQCIDG:$PC_{71}BM$-based hole-only devices.

The hole only devices fabricated with the structure of ITO (170 nm)/PEDOT:PSS(40 nm)/polymer:$PC_{71}BM$(34-110 nm)/MoO_3(30 nm)/Al(100 nm). Hole mobility measured in the films of PQCDPP:$PC_{71}BM$(1:5) and PQCIDG:$PC_{71}BM$ (1:3) using the space charge limited current model was 1.54×10^{-2} and 5.62×10^{-3} $cm^2(V^{-1}s^{-1})$, (mean from 8 devices) respectively, showing a high hole mobility owing to molecular planarity.

The reproducibility of the measured mobility is good from device to device and batch to batch as reflected by the small standard deviation.

In solid states, polymers with linear backbone chains have strong intermolecular π–π interactions and ordered packing.

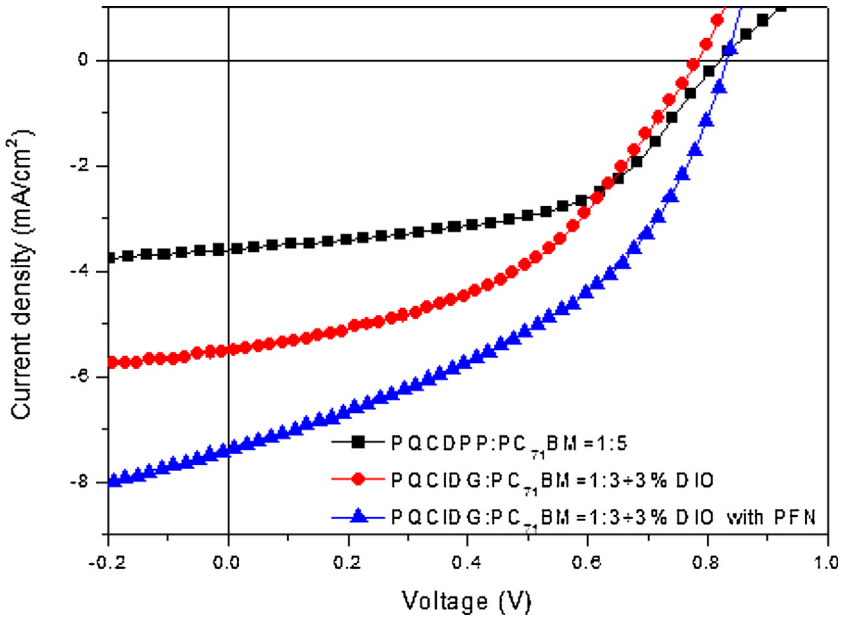

Fig. 6. *J–V* characteristics of the BHJ solar cells with the device.

Table 4
Photovoltaic performance of the BHJ solar cells.

Polymer	Solvent	weight ratio (w/w)	V_{oc} (V)	J_{sc} (mA/cm^2)	Calc. J_{sc} (mA/cm^2)	FF (%)	PCE[a,b] (%)
PQCDPP	ODCB	1:4	0.82	3.1	2.8	54.1	1.35 (1.4)
		1:5	0.83	3.6	3.4	52.9	1.59 (1.6)
	CB + 3% DIO	1:5	0.79	3.3	2.9	54.0	1.37 (1.4)
PQCIDG	ODCB	1:2	0.79	2.3	1.8	56.0	0.98 (1.0)
		1:3	0.81	3.3	2.9	49.5	1.26 (1.3)
	CB + 3% DIO	1:3	0.79	5.2	4.9	46.4	1.9 (1.9)
		1:3 with MeOH	0.82	5.9	5.6	49.5	2.3 (2.4)
		1:3 with PFN	0.83	7.4	7.2	43.1	2.65 (2.7)

[a] Mean solar cells with standard deviation from 8 devices of at least two batches for each fabrication condition.
[b] The value in parentheses is the highest solar cells observed.

3.7. Photovoltaic characteristics

In Fig. 6 and Table 4, the performance of OPV devices fabricated with the structure of ITO (170 nm)/PEDOT:PSS (40 nm)/active-layer (50 nm)/Al (100 nm). The 50–60 nm active layers were deposited by spin coating after the materials of polymer, phenyl C71-butyric acid methyl ester ($PC_{71}BM$) at different weight ratios were dissolved in *o*-dichlorobenzene, CB + 3% DIO.

The PQCDPP-based device (polymer/$PC_{71}BM$ = 1:5) showed a maximum PCE of 1.6% with V_{oc} 0.83, J_{sc} 3.6 mA/cm^2 and FF 52.9%.

The PQCIDG-based device (polymer/$PC_{71}BM$ = 1:3) showed a maximum PCE of 1.3% with V_{oc} 0.81 V, J_{sc} 3.3 mA/cm^2 and FF 49.5%.

In comparison to the performance of the thin films prepared with solvent additives of 1,8-DIO and chlorobenzene (CBz) with ODCB-treated films, the PQCIDG films showed an improvement in J_{sc}. However, the PQCDPP films did not show better efficiency than ODCB-treated films.

The effect of MeOH treatment of the active layer on the flatness of the backbone was also investigated. The MeOH treatment slightly improved the efficiency of the devices in terms of $V_{oc}J_{sc}$ and FF, leading to a PCE increase from 1.9% to 2.4%.

Recently, poly [(9,9-bis(30-(*N*,*N*-dimethylamino) propyl)-2,7-fuorene)-alt-2,7-(9,9-dioctylfuorene)] (PFN) is increasingly used to improve device efficiency owing to its ability to increase electron transport between the active layer and cathodes and interfacial adhesion. In this study, we incorporated PFN and a 1:3 ratio of PQCIDG/PC**71**BM into the device. The fabricated device comprised ITO/PEDOT:PSS/active layer(PQCIDG:PC71BM1:3with DIO)/Al and showed PCE of 1.9% with V_{oc}, J_{sc} and FF of 0.79 V, 7.4 mA cm2 and 46.4%, respectively. When the device was fabricated with a different structure of ITO/PEDOT:PSS/active layer (PQCIDG: PC71BM 1:3 with DIO)/PFN/Al, it showed PCE of 2.7% with V_{oc}, J_{sc} and FF of 0.83 V, 7.4 mA cm2 and 43.1%, respectively. Thus, PFN incorporation led to better device efficiency by means of improving V_{oc} and J_{sc}.

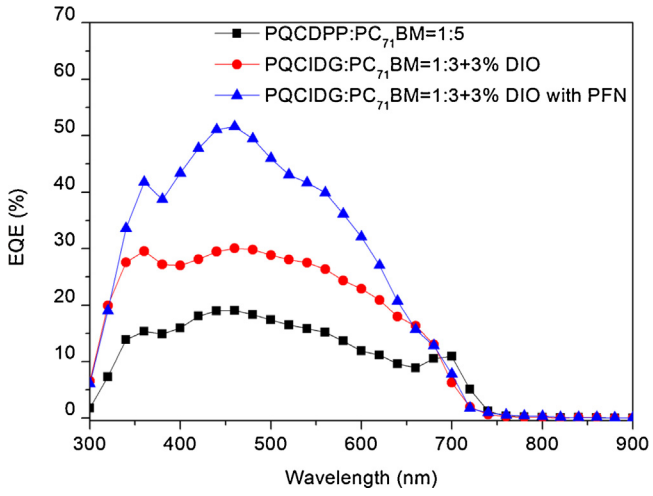

Fig. 7. EQE spectra of the solar cells with the device.

To ensure accuracy of the measurement, the external quantum efficiency (EQE) of solar cells was measured, and EQE curves of the maximum efficiency of cells were described. The photons in the EQE curve occurred mostly in the polymer phase, which correlated with the absorption spectra of the polymers [38]. As shown in Fig. 7, the PQCDPP-based device showed a wide EQE curve in the wavelength range of 300–740 nm, and the PQCIDG-based device also showed a strong absorbance in the region of 300–700 nm [17,27].

3.8. Morphology analysis

The surface morphology of the polymer/PCBM film was measured using atomic force microscopy. As shown in Fig. 8(a) and (b), the PQCDPP/PCBM films showed macrophase domains whereas the PQCDPP/PCBM films with DIO showed island domains, which interferes with the exciton separation and lowers J_{sc}.

By contrast, the DIO-treated PQCIDG/PCBM films showed more fibril-like domains as shown in Fig. 8 (c) and (d), creating a new pathway in the ordered region for charge transport through long polymer backbones [39]. Improved carrier mobility led to an improvement in the J_{sc} value of the respective devices and current-data of the IPCE.

4. Conclusions

We successfully synthesized two novel polymers using QC as the weak donor and DPP and IDG as the strong acceptor via the Suzuki coupling reaction.

The synthetic polymers were characterized by high solubility (the effect of *N*-alkylation), and molecular weight and thermal stability. Also, these polymers maintained their charge balance and low band of 1.92 by the combined effects of proper HOMO and LUMO energy. The PQCDPP- and PQCIDG-based film exhibited a wide absorption spectra of 350–750 nm, which originated from the π–π^* transition of conjugated backbones and a strong intramolecular charge transfer. PQCDPP- and PQCDIG-based films exhibited high flatness, broad diffraction peaks in the XRD pattern around 24.0 and 24.5°, respectively, and the π–π stacking distance (d_π) of 3.61, 3.63 Å, respectively, showing a significantly short

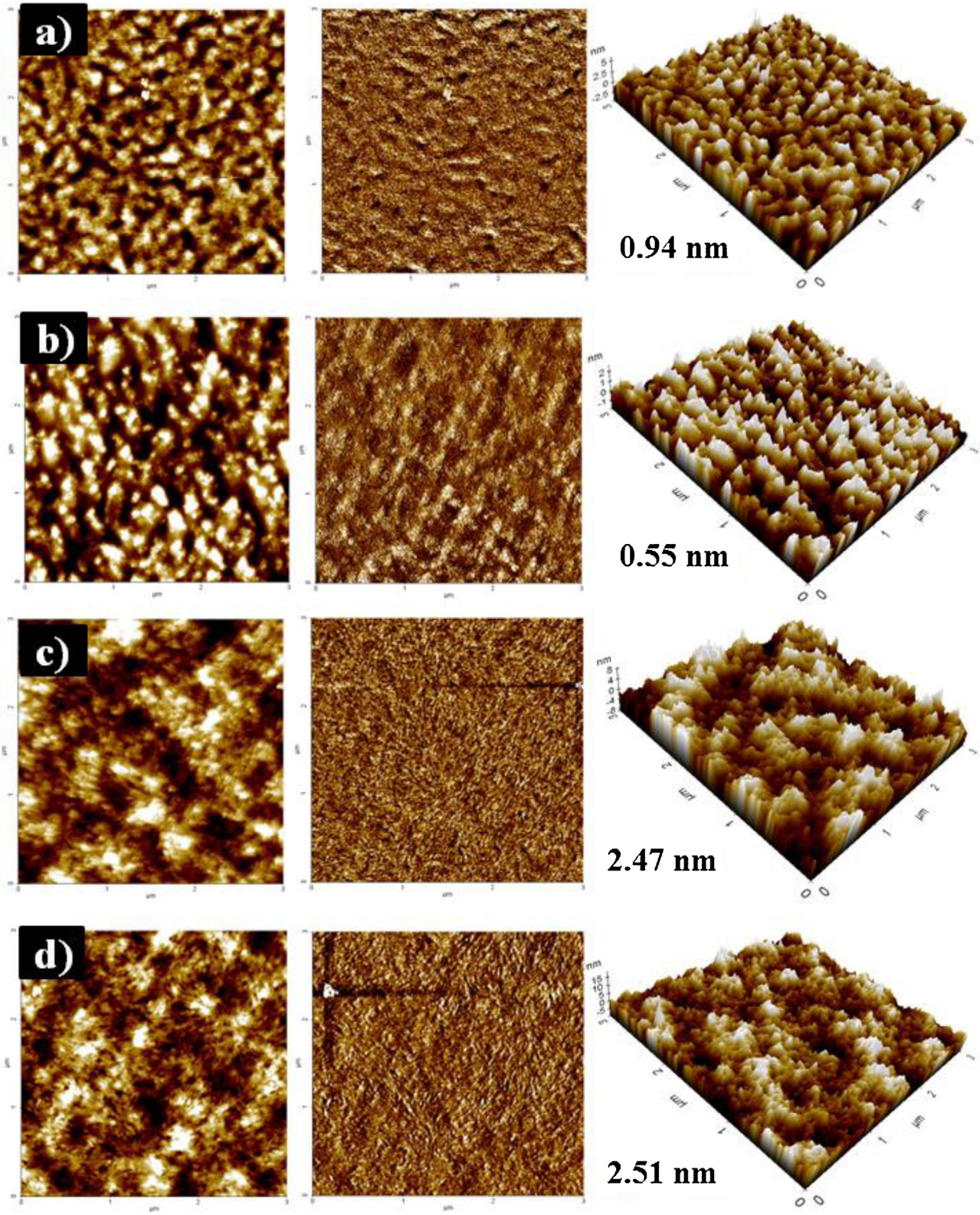

Fig. 8. Topographic AFM images of PQCDPP:$PC_{71}BM$ = 1:5 (a) oDCB (b) CB with DIO and PQCIDG:$PC_{71}BM$ = 1:3 (c) oDCB (d) CB with DIO. The imaging size is $3 \times 3\ \mu m^2$ for each panel: height images (left and right) and phase images (center).

distance in agreement with the pre-existing values of polymers derived from thiophene and thiophene-fused aromatic systems. In addition, PQCDIG-based films exhibited a face-on and vertical orientation of crystallinity by allowing a strong π–π interaction and effective transport of electrons and holes.

The PQCIDG in CBz + DIO films (polymer/$PC_{71}BM$ = 1:3) resulted in an improved PCE of 2.7% with V_{oc} of 0.83 V, J_{sc} of 7.4 mA/cm^2 and FF of 43.1%.

Acknowledgements

This research was supported by the National Research Foundation of Korea Grant funded by the Korean Government (MEST) (NRF-2012M1A2A2671703) and by the New & Renewable Energy Core Technology Program of the Korea Institute of Energy Technology Evaluation and Planning (KETEP) grant funded by the Ministry of Trade, industry & Energy (MI, Korea) (no. 20133030000180).

Appendix A. Supplementary data

Supplementary data associated with this article can be found, in the online version, at http://dx.doi.org/10.1016/j.synthmet.2015.10.009.

References

[1] W. Lu, J. Kuwabara, T. Kanbara, Polycondensation of dibromofluorene analogues with tetrafluorobenzene via direct arylation, Macromolecules 44 (2011) 1252–1255.
[2] R.H. Friend, R.W. Gymer, A.B. Holmes, J.H. Burroughes, R.N. Marks, C. Taliani, D. D.C. Bradley, D.A.D. Santos, J.L. Bredas, M. Logdlund, W.R. Salaneck, Electroluminescence in conjugated polymers, Nature 397 (1999) 121–128.
[3] H.J. Song, G.J. Shin, K.H. Choi, S. Lee, D.K. Moon, White polymer light emitting diode materials introducing dendritic quinoxaline derivative: Synthesis, optical and electroluminescent properties, Synth. Met. 190 (2014) 1–7.
[4] Z.C. He, C.M. Zhong, S.J. Su, M. Xu, H.B. Wu, Y. Cao, Enhanced power-conversion efficiency in polymer solar cells using an inverted device structure, Nat. Photonics 6 (2012) 591–595.
[5] K.W. Song, M.H. Choi, J.Y. Lee, D.K. Moon, Opto-electrical and density functional theory analysis of poly(2,7-carbazole-alt-thieno[3,4-c]pyrrole-4,6-dione) and photovoltaic behaviors of bulk heterojunction structure, J. Ind. Eng. Chem. 20 (2014) 290–296.
[6] K.W. Song, M.h. Choi, M.h. Han, D.K. Moon, Open circuit voltage increase by substituted spacer and thieno[3,4-c]pyrrole-4,6-dione for polymer solar cells, J. Ind. Eng. Chem. 20 (2014) 426–434.
[7] H.J. Song, D.H. Kim, E.J. Lee, J.R. Haw, D.K. Moon, Correlation of intramolecular charge transfer and orientation properties among quinacridone and acceptor units, Sol. Energy Mater. Sol. Cells 123 (2014) 112–121.
[8] J.Y. Lee, H.J. Song, S.M. Lee, J.H. Lee, D.K. Moon, Synthesis and investigation of photovoltaic properties for polymer semiconductors based on porphyrin compounds as light-harvesting units, Eur. Polym. J. 47 (2011) 1686–1693.
[9] I. Osaka, K. Takimiya, Backbone orientation in semiconducting polymers, Polymer 59 (2015) A1–15.
[10] T. Yasuda, Y. Sakai, S. Aramaki, T. Yamamoto, New coplanar (ABA) *n*-type donor–acceptor π-conjugated copolymers constituted of alkylthiophene (Unit A) and pyridazine (Unit B): synthesis using hexamethylditin, self-organized solid structure, and optical and electrochemical properties of the copolymers, Chem. Mater. 17 (2005) 6060–6068.
[11] Y. Cao, Z.-H. Guo, Z.-Y. Chen, J.-S. Yuan, J.-H. Dou, Y.-Q. Zheng, J.-Y. Wang, J. Pei, Pentacyclic aromatic bislactam-based conjugated polymers: constructed by Beckmann rearrangement and application in organic field-effect transistor, Polym. Chem. 5 (2014) 5369–5374.
[12] D. Dang, P. Zhou, J. Zhong, J. Fan, Z. Wang, Y. Wang, Y. Pei, X. Bao, R. Yang, W. Hu, W. Zhu, Novel wide band-gap polymer utilizing fused hetero-aromatic unit for efficient polymer solar cells and field-effect transistors, Polymer 55 (2014) 6708–6716.
[13] J.Y. Lee, W.S. Shin, J.R. Haw, D.K. Moon, Low band-gap polymers based on quinoxaline derivatives and fused thiophene as donor materials for high efficiency bulk-heterojunction photovoltaic cells, J. Mater. Chem. 19 (2009) 4938–4945.
[14] D. Cao, Q. Liu, W. Zeng, S. Han, J. Peng, S. Liu, Diketopyrrolopyrrole-containing polyfluorenes: facile method to tune emission color and improve electron affinity, Macromolecules 39 (2006) 8347–8355.
[15] J.C. Bijleveld, A.P. Zoombelt, S.G.J. Mathijssen, M.M. Wienk, M. Turbiez, D.M. de Leeuw, R.A.J. Janssen, Poly(diketopyrrolopyrrole-terthiophene) for ambipolar logic and photovoltaics, J. Am. Chem. Soc. 131 (2009) 16616–16617.
[16] P. Deng, Q. Zhang, Recent developments on isoindigo-based conjugated polymers, Polym. Chem. 5 (2014) 3298–3305.
[17] F. Liu, Y. Gu, C. Wang, W. Zhao, D. Chen, A.L. Briseno, T.P. Russell, Efficient polymer solar cells based on a low bandgap semi-crystalline DPP polymer-PCBM blends, Adv. Mater. 24 (2012) 3947–3951.
[18] A.R. Han, G.K. Dutta, J. Lee, H.R. Lee, S.M. Lee, H. Ahn, T.J. Shin, J.H. Oh, C. Yang, ε-Branched flexible side chain substituted diketopyrrolopyrrole-containing polymers designed for high hole and electron mobilities, Adv. Funct. Mater. 25 (2015) 247–254.
[19] Z. Wang, J. Zhao, Y. Li, Q. Peng, Low band-gap copolymers derived from fluorinated isoindigo and dithienosilole: synthesis, properties and photovoltaic applications, Polym. Chem. 5 (2014) 4984–4992.
[20] I. Osaka, M. Akita, T. Koganezawa, K. Takimiya, Quinacridone-based semiconducting polymers: implication of electronic structure and orientational order for charge transport property, Chem. Mater. 24 (2012) 1235–1243.
[21] H.-J. Song, D.-H. Kim, E.-J. Lee, S.-W. Heo, J.-Y. Lee, D.-K. Moon, Conjugated polymer consisting of quinacridone and benzothiadiazole as donor materials for organic photovoltaics: coplanar property of polymer backbone, Macromolecules 45 (2012) 7815–7822.
[22] M.-H. Choi, K.W. Song, D.K. Moon, Alkylidenefluorene-isoindigo copolymers with an optimized molecular conformation for spacer manipulation, [small pi-small pi] stacking and their application in efficient photovoltaic devices, Polym. Chem. 6 (2015) 2636–2646.
[23] H.J. Song, S.M. Lee, J.Y. Lee, B.H. Choi, D.K. Moon, The synthesis and electroluminescent properties of dithienylquinacridone-based copolymers for white light-emitting diodes, Synth. Met. 161 (2011) 2451–2459.
[24] L. Dou, J. Gao, E. Richard, J. You, C.-C. Chen, K.C. Cha, Y. He, G. Li, Y. Yang, Systematic investigation of benzodithiophene- and diketopyrrolopyrrole-based low-bandgap polymers designed for single junction and tandem polymer solar cells, J. Am. Chem. Soc. 134 (2012) 10071–10079.
[25] Z. Ma, W. Sun, S. Himmelberger, K. Vandewal, Z. Tang, J. Bergqvist, A. Salleo, J. W. Andreasen, O. Inganas, M.R. Andersson, C. Muller, F. Zhang, E. Wang, Structure-property relationships of oligothiophene-isoindigo polymers for efficient bulk-heterojunction solar cells, Energy Environ. Sci. 7 (2014) 361–369.
[26] J.D. Yuen, F. Wudl, Strong acceptors in donor-acceptor polymers for high performance thin film transistors, Energy Environ. Sci. 6 (2013) 392–406.
[27] Z. Zeng, Y. Li, J. Deng, Q. Huang, Q. Peng, Synthesis and photovoltaic performance of low band gap copolymers based on diketopyrrolopyrrole and tetrathienoacene with different conjugated bridges, J. Mater. Chem. 2 (2014) 653–662.
[28] T. Lei, Y. Cao, X. Zhou, Y. Peng, J. Bian, J. Pei, Systematic investigation of isoindigo-based polymeric field-effect transistors: design strategy and impact of polymer symmetry and backbone curvature, Chem. Mater. 24 (2012) 1762–1770.
[29] M. Akita, I. Osaka, K. Takimiya, Quinacridone-diketopyrrolopyrrole-based polymers for organic field-effect transistors, Materials 6 (2013) 1061–1071.
[30] J. Hou, T.L. Chen, S. Zhang, L. Huo, S. Sista, Y. Yang, An easy and effective method to modulate molecular energy level of poly(3-alkylthiophene) for high-voc polymer solar cells, Macromolecules 42 (2009) 9217–9219.
[31] D.H. Kim, H.J. Song, S.W. Heo, K.W. Song, D.K. Moon, Enhanced photocurrent generation by high molecular weight random copolymer consisting of benzothiadiazole and quinoxaline as donor materials, Sol. Energy Mater. Sol. Cells A 120 (2014) 94–101.
[32] C. Piliego, T.W. Holcombe, J.D. Douglas, C.H. Woo, P.M. Beaujuge, J.M.J. Fréchet, Synthetic control of structural order in *N*-alkylthieno[3,4-c]pyrrole-4,6-dione-based polymers for efficient solar cells, J. Am. Chem. Soc. 132 (2010) 7595–7597.
[33] H.-J. Song, D.-H. Kim, E.-J. Lee, D.-K. Moon, Conjugated polymers consisting of quinacridone and quinoxaline as donor materials for organic photovoltaics: orientation and charge transfer properties of polymers formed by phenyl structures with a quinoxaline derivative, J. Mater. Chem. A 1 (2013) 6010–6020.
[34] M.-H. Choi, E.J. Ko, Y.W. Han, E.J. Lee, D.K. Moon, Control of polymer-packing orientation in thin films through chemical structure of D–A type polymers and its application in efficient photovoltaic devices, Polymer 74 (2015) 205–215.
[35] S. Subramaniyan, H. Xin, F.S. Kim, S. Shoaee, J.R. Durrant, S.A. Jenekhe, Effects of side chains on thiazolothiazole-based copolymer semiconductors for high performance solar cells, Adv. Energy Mater. 1 (2011) 854–860.
[36] J. Guo, Y. Liang, J. Szarko, B. Lee, H.J. Son, B.S. Rolczynski, L. Yu, L.X. Chen, Structure, dynamics, and power conversion efficiency correlations in a new low bandgap polymer: PCMB solar cell, J. Phys. Chem. B 114 (2010) 742–748.
[37] J. Rivnay, M.F. Toney, Y. Zheng, I.V. Kauvar, Z. Chen, V. Wagner, A. Facchetti, A. Salleo, Unconventional face-on texture and exceptional in-plane order of a high mobility n-type polymer, Adv. Mater. 22 (2010) 4359–4363.
[38] J.Y. Lee, S.H. Kim, I.S. Song, D.K. Moon, Efficient donor-acceptor type polymer semiconductors with well-balanced energy levels and enhanced open circuit voltage properties for use in organic photovoltaics, J. Mater. Chem. 21 (2011) 16480–16487.
[39] R.J. Kline, M.D. McGehee, E.N. Kadnikova, J. Liu, J.M.J. Fréchet, M.F. Toney, Dependence of regioregular poly(3-hexylthiophene) film morphology and field-effect mobility on molecular weight, Macromolecules 38 (2005) 3312–3319.